Volume 48
Number 40
28 October 2024
Pages 17365–17678

# NJC

New Journal of Chemistry

A journal for new directions in chemistry

rsc.li/njc

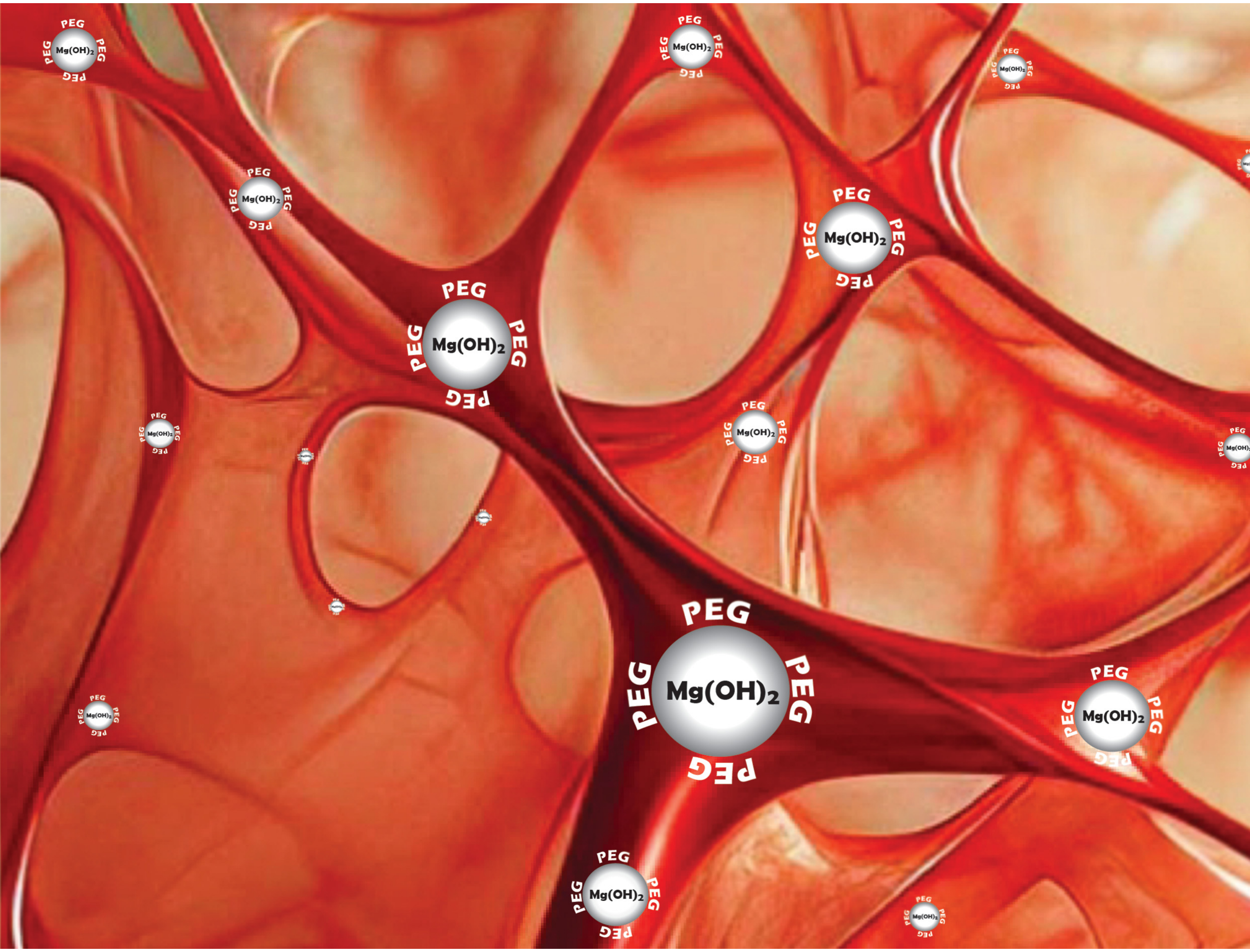

ISSN 1144-0546

ROYAL SOCIETY OF **CHEMISTRY**

**PAPER**
Yasir Javed, Nguyen Thi Kim Thanh *et al.*
Polymer coated magnesium hydroxide nanoparticles for enhanced wound healing

NJC

ROYAL SOCIETY OF CHEMISTRY

PAPER

View Article Online
View Journal | View Issue

Check for updates

Cite this: *New J. Chem.*, 2024, **48**, 17396

Received 25th April 2024,
Accepted 5th August 2024

DOI: 10.1039/d4nj01909a

rsc.li/njc

# Polymer coated magnesium hydroxide nanoparticles for enhanced wound healing†

Muhammad Khawar Abbas,[ab] Yasir Javed,*[b] Naveed Akhtar Shad,[c] Muhammad Shahid,[d] Bushra Akhtar,[e] Effat Yasin,[ab] Surender Kumar Sharma[f] and Nguyen Thi Kim Thanh*[gh]

Wound healing potential is initially evaluated using a chorioallantoic membrane (CAM) assay. Alginate gel containing pristine and polymer-coated magnesium hydroxide nanoparticles (MHNPs) improves the healing response. PEGylated MHNPs have shown a rapid wound-healing process in *Gallus gallus domesticus* by promoting re-epithelialization as compared to pristine MHNPs. No toxicity or inflammation are observed in the blood, liver, and heart tissues during biochemistry and histopathological examination. Polymer (polyethylene glycol (PEG) and chitosan) functionalized MHNPs are synthesized using a one-step hydrothermal process. The average crystallite size determined from X-ray diffraction analysis of the pristine MHNPs is ~31.3 nm and upon PEG and chitosan coating it reduces to 23.4 nm and 29.7 nm, respectively. FTIR confirms the presence of functional groups indicating the successful functionalization of the polymers.

## 1. Introduction

In recent years, pathogens have been treated with metal and metal oxide NPs, which offer broad-spectrum antibacterial properties.[1] Metal and metal oxide-based NPs have proven strong antibacterial potential both in preclinical and clinical therapeutic trials.[2] The mode of action of NPs while attacking bacterial and cancerous cells is different as compared to medicinal drugs. The exact mechanism adopted by NPs has not yet been elucidated.[3] However, it is assumed that they follow the model of introducing oxidative stress, localized discharge of metallic cations, immediate interaction with microbial cell walls, or intracellular disruption of organelles.[4,5] The suitable choice of polymer increases the stability, minimizes the aggregation of NPs and improves the inherent properties of NPs.[6] Surface modifications of metal oxide NPs with various natural or synthetic polymers are considered a tuning factor for sorption behaviors, redox reactions, changing surface chemistry, and controlling band gaps.[7–10] PEG and chitosan are FDA-approved polymers and widely used in many biomedical applications. The conjugation of PEG with NPs is associated with the presence of a chemically active OH group at its linear ends and diverse functional groups at the surface of the NPs.[11–14] PEG coating suppresses the immune response by an opsonization process and in this way the retention time or blood circulation time of a drug or NPs in a biological system increases.[15] Chitosan is the second most abundant polymer after cellulose.[16] The protonation ability of chitosan gives a positive charge on the surface of the NPs[17] and can be effective against microbes that modulate the wound healing process.[18,19]

Skin is the largest organ that separates the internal body medium from the external environment. It functions as a first line of defense between harmful pathogens and internal body organs. In this way, it maintains the internal bodily homeostasis. Wounds appear in the case of serious skin disruption; chronic wounds can have negative impacts on health and affect the quality of life.[20] Wound healing is a complicated and ongoing process, completed in a series of phases to restore the physical integrity of damaged cells.[21,22] In the case of poor hygienic conditions, infectious bacteria like *Escherichia coli* (*E. coli*) and *Staphylococcus aureus* (*S. aureus*) settle down at the wound site and can cause active infection by interfering with the wound healing process. These bacteria discharge various endotoxins, *i.e.* lipopolysaccharides (*E. coli*) and TSS-1 (*S. aureus*),[23,24] that can induce fibrin and collagen lysis and slow down the proliferation of fibroblasts and epithelial cells.[25] Bacteria consume more oxygen and nutrients at the expense

---

[a] *Department of Physics, Government College University Faisalabad, Faisalabad, Pakistan*

[b] *Department of Physics, University of Agriculture, Faisalabad, Pakistan. E-mail: yasir.javed@uaf.edu.pk*

[c] *National Institute of Biotechnology and Genetic Engineering, Jhang Road, Faisalabad, Pakistan*

[d] *Department of Biochemistry, University of Agriculture, Faisalabad, Pakistan*

[e] *Department of Pharmacy, University of Agriculture, Faisalabad, Pakistan*

[f] *Department of Physics, Central University of Punjab, Bathinda, 151401, India*

[g] *Biophysics group, Department of Physics and Astronomy, University College London, Gower Street, London WC1E 6BT, UK. E-mail: ntk.thanh@ucl.ac.uk*

[h] *UCL Healthcare Biomagnetics and Nanomaterials Laboratories, 21 Albemarle Street, London W1S 4BS, UK*

† Electronic supplementary information (ESI) available. See DOI: **https://doi.org/10.1039/d4nj01909a**

of newly formed tissues, which degrades growth factors. This situation leads to tissue anoxia and thus healing of wounds is further delayed.[26] Therefore, applying a strong antibacterial agent on the wound bed which can inhibit the growth of bacteria without damaging the healthy cells is necessary to accelerate the natural healing process of the body.[27]

Although nanoparticles have shown promising results in wound healing trials, toxicity, *in vivo* efficacy, scalability, and regularity approval from the FDA are major issues that need to be resolved for advanced research.[28] Magnesium hydroxide is bio-safe. The FDA has recommended $Mg(OH)_2$ as a GRAS (generally recognized as safe) ingredient and pH control agent in food and nutritional supplements.[29] MHNPs are biocompatible and included in many pharmaceutical products due to their antibacterial action.[30,31] The growth inhibition of both $G^+$ and $G^-$ bacterial strains is reported by exposing them to MHNPs. The strong antimicrobial and biofilm inhibition actions are associated with the ability of MHNPs to produce a highly localized alkaline environment. Such an environment lowers the production of adenosine triphosphate molecules by consuming local $H^+$, which results in an energy deficit and consequently limits the microbial cellular metabolism.[32,33] The small size of NPs improves the cell internalization process and consequently favors antimicrobial action.[34] Halbus *et al.* reported that the bactericidal properties of MHNPs are found in inverse relation to the particle size.[5] The MHNPs accelerate the recovery of wounds by preventing bed sores during the healing process.[35] Firstly, the process involves the anti-inflammatory action of $Mg^{2+}$ ions. Secondly, the pro-angiogenic action of MgO in speeding up the healing process is linked with the expression of vascular endothelial growth (VEGF), which triggers angiogenesis, increases the number of blood vessels, and carries more nutrients to the wounded area.[36] Thirdly, differentiation and proliferation of endothelial cells are stimulated. It increases the production of IL-12 secreted by neutrophils, which reduces the duration of reepithelization.[37] Lastly, the strong antibacterial action of MHNPs towards pyogenic pathogens can increase the chronicity of wounds, making it a good wound-healing agent. Colloidal instability, early biodegradation, and aggregation of MHNPs limit their effectiveness; in the case of PEGylation, the PEG molecule remains over the surfaces of the NPs without entering into the core structure and thus can enhance the shelf life of the NPs,[38,39] and in this way, potential biological applications of MHNPs can be optimized.

In the present work, pristine, PEG, and chitosan-functionalized MHNPs are synthesized using a one-step hydrothermal process. The pristine and polymer-coated nano-systems are characterized by X-ray diffraction (XRD), scanning electron microscopy (SEM), Fourier-transform infrared (FTIR) spectroscopy, photoluminescence[12] spectroscopy, ultraviolet-visible spectroscopy (UV-vis spectroscopy) and dynamic light scattering (DLS). The wound healing potential of the pristine and surface-functionalized MHNPs is evaluated using CAM assay and *in vivo* (*G. domesticus*). To further understand the process, the antimicrobial response is evaluated on bacterial stains and biofilm inhibition.

## 2. Experimental section

### 2.1 Chemicals

The magnesium salt (magnesium nitrate hexahydrate ($Mg(NO_3)_2\cdot 6H_2O$; DAEJUNG, Korea 98%)), PEG-6000 (DAEJUNG, Korea), chitosan (Icon Chemicals, Germany 90%), and NaOH pellets (Icon Chemicals, Germany 98%) were utilized as received.

### 2.2 Synthesis of magnesium hydroxide NPs

MHNPs were synthesized by applying a one-step hydrothermal route. The experimental details were as follows: 0.5 M salt ($Mg(NO_3)_2\cdot 6H_2O$) solution and 1 M base (NaOH) solution were prepared separately in 100 mL distilled water. Then the base solution was added to the salt solution very slowly (drop-wise) under vigorous magnetic stirring. To increase the homogeneity, the final mixture was sonicated for 30 min. Afterwards, the uniform mixture was put into Teflon-lined autoclaves and placed into an oven for 16 h at 180 °C. Then the reaction mixture was centrifuged to obtain the precipitates and washed in triplicate with distilled water to eliminate any by-products. The precipitates were placed in the oven overnight at 80 °C and then the dried precipitates were ground to powder form. Similarly, 0.1 g of PEG and chitosan were added separately to the reaction mixture and stirred for 30 min more before putting the salt solution into the Teflon-lined autoclave for hydrothermal treatment.[40]

### 2.3 Characterization tools

For structure analysis of bare and polymer functionalized MHNPs, XRD (D8 Advance-Bruker) in the $2\theta$ range of 20 to 60° was used. Grain morphology was studied by SEM (NOVA NanoSEM). Surface chemistry was evaluated by FTIR (Agilent Technologies, Cary 630 FTIR). Energy band and optical behavior were determined by UV-vis spectrophotometer and PL spectra. The thermal stability of the pristine, PEGylated, and chitosan functionalized MHNPs was studied using the differential scanning calorimetry-thermogravimetric analysis (DSC-TGA) standard module using SDT Q600 V20.9 Build 20 under $N_2$. Dynamic light scattering (DLS) was performed to determine the hydrodynamic size of the NPs using Zetasizer Ver. 7.11 Serial Number: MAL 1127001 (Malvern Inc). The students' *t*-test was applied to analyze the data statistically.

### 2.4 Antibacterial and biofilm inhibition assessment

The Kirby Bauer disk diffusion susceptibility protocol was employed to study the antibacterial activity of the nanomaterials for *S. aureus* and *E. coli* bacteria.[41] Experiments for both antibacterial action and biofilm inhibition percentage were performed by following the protocols previously reported.[42]

### 2.5 Hemolysis percentage assessment

After written consent and taking ethical permission from university's ethical committee, 10 mL of human blood samples were taken from healthy donors in citrated or heparinized tubes (3.8% sodium citrate or lithium heparin).[43] Then a mixture of 3 mL blood cells and 15 mL polystyrene was centrifuged for 5 min. For pH stability, the viscous pellets were washed in triplicate with a 5 mL sterile solution of isotonic phosphate buffer saline (PBS), maintained at 4 °C for 1 h. In this way, the cells were washed and then suspended in chilled and sterile PBS having a final volume of 20 mL. The suspension was kept in ice and diluted with sterile PBS to $7.068 \times 10^8$ cells per mL. Three sets of 20 mL solutions of MHNPs, PEG-coated MHNPs, and chitosan-coated MHNPs were formed. Triton X-100 and PBS were the positive and negative controls, respectively. The remaining 180 μL diluted blood cell suspension was kept aseptically in a 2 mL tube. The nanomaterial concentration was kept at 250 $\mu$mol L$^{-1}$. The sample holding tubes were incubated for 30 min at 37 °C with a shaking speed of 80 rpm. Then the tubes were put in wet ice for 5 min and again centrifuged for 5 min. The samples were carefully collected and placed into a 1.5 mL tube where they were diluted with 900 μL of sterile and chilled PBS. Finally, all the tubes were kept in wet ice.[44] For validation, three replicates were performed for each nanomaterial sample. Absorbance at wavelength 576 nm was determined by Bausch and Lomb Spectronic 1001 spectrometer using a quartz cuvette. A hemocytometer (Fisher ultra plane, Neubauer ruling) was used to count the cells. The percentage of hemolysis was determined by using eqn (1):

$$\%\ \text{Hemolysis} = \frac{\text{Sample absorbance} - \text{Negative control absorbance}}{\text{Positive control absorbance} - \text{Negative control absorbance}} \times 100. \tag{1}$$

### 2.6 Wound healing properties

**2.6.1 CAM assay.** The wound healing potential of pristine, PEG, and chitosan-coated MHNPs was evaluated using a CAM assay. Commercial alginate gel was composited with NPs by dipping the gel in a 200 mg suspension of NPs for 15 min. Fertilized eggs (chickens) were purchased from a local poultry farm; all the eggs were thoroughly cleaned with distilled water and ethanol. Then they were placed in an incubator at 37 °C in a humid environment. After a week, 1.5 square inch shells from each egg were detached by a sterile surgical cutter. Then the cut part of the egg shells was covered with the composite gel. The gels were removed on the 15th day to observe the ongoing growth of the chicks and photographs were taken. Control eggs were pasted with alginate gel only.[45]

**2.6.2 Swelling properties.** The swelling properties of alginate gel and alginate gel impregnated with MHNPs were studied by immersing the gels in a 3 M brine solution for different durations. The weight differences of the gels; wet gel ($W_{\text{wet}}$) and dry gel ($W_{\text{dry}}$) were obtained after 15 min, 30 min, 1 h, 2 h, 3 h, 4 h, 5 h, and 24 h. The swelling percentage was determined using eqn (2).[46]

$$\%\ \text{Swelling} = \frac{W_{\text{wet}} - W_{\text{dry}}}{W_{\text{dry}}} \times 100. \tag{2}$$

**2.6.3 *In vivo* wound healing study.** The wound healing potential of the pristine, PEGylated, and chitosan-functionalized MHNPs was also studied by applying an open excision type cut/wound on the peritoneal side of *G. domesticus*. Fifteen-day-old healthy chickens (female) were taken from the local poultry farm. The birds were put in the disinfected cage under a suitable temperature of 25 ± 3 °C for a couple of days and were fed properly to acclimatize them to the laboratory environment, then they were divided into groups as given in Table 1. Each group contains three animals. The birds were anesthetized with inter-breast injection for a short time by the mixture of ketamine (20 mg kg$^{-1}$) live weight and xylazine (2 mg kg$^{-1}$).[47] After removing/shaving feathers from the excision point, the skin of each bird was cleaned with spirit; a 25 mm long (linear) cut/wound was given to the birds on the peritoneal side to the depth of loose subcutaneous tissues with a sterile surgical blade.[48] In control-1 the wounds were treated daily with Vetericyne Plus®, a commonly available antimicrobial poultry care spray, whereas control-2 were not given any treatment and their wounds were observed to heal naturally. The wounds of groups A, B, and C were sprayed daily with the suspension of 10 g L$^{-1}$ pristine, PEG, and chitosan-coated MHNPs, respectively.[49,50] All the birds were handled gently to minimize the stress; the appearances and healing of the wounds were photographed regularly for 9 d both in the morning and evening. The healing rate was calculated using eqn (3):

$$\text{Wound area} = \frac{A_{\text{t}}}{A_{\text{o}}} \times 100 \tag{3}$$

Here, $A_{\text{o}}$ is the area of the wound on the day of operation and $A_{\text{t}}$ is the area on a specified day.[51,52]

## 3. Results and discussion

### 3.1 Synthesized material analysis

XRD is used as a characterization technique for the structural analysis of the synthesized nanomaterials. XRD patterns of pristine and polymer-functionalized MHNPs are shown in Fig. 1.

The formation of single-phase MHNPs is confirmed by XRD with pdf # 01-074-2220 showing the hexagonal structure and belonging to the space group $P\bar{3}m1$. Four diffraction peaks are observed at positions 32.8°, 38°, 50.8°, and 58.6° which correspond to the (100), (101), (102), and (110) planes respectively in bare MHNPs. The PEG and chitosan functionalized MHNP patterns have identical behavior; however, the peaks at 38° and 50.8° are minutely shifted towards a lower angle, which may be attributed to the attachment of organic polymer during the reaction, subsequently changing the nanoparticle characteristics. The polymer coating has also shown effects on the structural parameters, which varied as compared to bare MHNPs (Table 2). Debye–Scherrer's relation is used to determine the crystallite size

Table 1 Grouping of chicks with their average weight and wound healing agent

| Group | Avg. weight (g) | Wound healing agent |
|---|---|---|
| Control-1 | 292 ± 5 | Vetericyne plus®, poultry care spray |
| Control-2 | 313 ± 4 | Natural healing |
| A | 295 ± 2 | MHNPs |
| B | 305 ± 2 | PEG-MHNPs |
| C | 307 ± 2 | Chitosan-MHNPs |

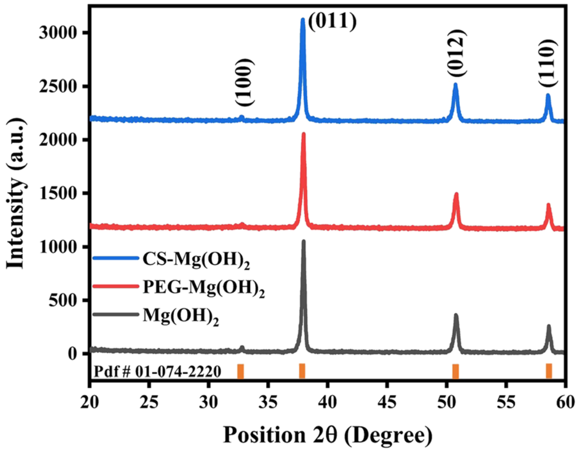

Fig. 1 XRD patterns of bare and polymer functionalized MHNPs.

(eqn (4)).

$$D = \frac{K\lambda}{\beta \cos\theta} \quad (4)$$

The crystallite size of MHNPs is 31.3 nm which is slightly reduced to 29.7 nm in the case of chitosan-coated MHNPs; however, PEG functionalized MHNPs have a much-reduced crystallite size (23.4 nm) and the distinct behavior of crystallite aggregation is observed during the growth process. This variable behavior may be associated with the charge of organic polymers as PEG is a neutral to negatively charged open-branched polymer and chitosan has a positive charge owing to the residual amino groups. This diversity in charge of polymers can certainly dictate crystal growth. Furthermore, these organic moieties can affect the morphology, shape, and size distribution of NPs. The lattice dimensions and cell volume remain almost the same for the three materials while the lattice strain and dislocation densities vary significantly for PEG and chitosan-coated MHNPs.

Texture coefficient (T.C.) is used to determine favorable planes in which the crystalline material shows a preferred tendency to grow. The T.C. is calculated by eqn (5).

$$\text{T.C.} = \frac{\left(\dfrac{I(hkl)}{I_o(hkl)}\right)}{\left(\dfrac{1}{N}\right)\sum I(hkl)/I_o(hkl)} \quad (5)$$

If the T.C. is less than unity (T.C. $< 1$), the growth direction will be random, and a value more than 1 represents the preferred growth direction of crystals. The plane having the highest value of T.C. indicates the favored direction for crystallite growth.[53] The MHNPs have the maximum value of T.C. for the (110) plane, indicating the thermo-dynamical possibility of crystalline growth along this direction. Whereas, when MHNPs are composited with PEG and chitosan, the favorable growth direction changes to (100) (Table 3).

It is believed that during the hydrothermal reaction, water molecules gradually decompose into solvated $H^+$ (hydrogen cations) and $OH^-$ (hydroxide anions) under heating and pressure. The increase in temperature plays a vital role in the degree of water dissociation. At room temperature, the magnesium nitrate hexahydrate is not affected too much by the water; however, when the solution is exposed to high temperature and pressure, the magnesium salt is decomposed into $Mg^{2+}$ cations and reacts with $OH^-$, leading to the formation of $Mg(OH)_2$. The detailed analysis of the mentioned chemical reactions shows that $MgOH^+$ ions, *i.e.* hydroxo-complexes of $Mg^{2+}$, contribute to the growth proceeding during the formation of magnesium hydroxide nanocrystals.[54]

Fig. 2(a) and (b) present the morphology and grain size of the MHNPs, the low and high magnification micrographs of MHNPs show spherical, hexagon, and rectangular-like grains with a mean size of 74 ± 17 nm (Fig. 2c). In the case of PEGylation of MHNPs, the shape of the grains is not much varied as compared to the pristine MHNPs (Fig. 2d and e), whereas grain size is determined as 72 ± 16 nm (Fig. 2f). Fig. 2 shows micrographs of chitosan-coated MHNPs where the mean size is reduced to 55 ± 13 nm (Fig. 2i). The *t*-test shows that the grain sizes of MHNPs and PEG–MHNPs are not statistically different with $p = 0.1007$ whereas the gain size of chitosan–MHNPs is statistically different than bare MHNPs ($p < 0.0001$). The grain size reduction is owing to the surface functionalization of MHNPs, where the polymer has controlled the coalescence of particles, and the composite formation of MHNPs with chitosan has lessened the atomic attachment during the grain growth process.[55] XRD results also confirmed the decrease in crystallite size when PEG and chitosan are coated on MHNPs.

The absorption bands are shown at 289 nm, 285 nm, and 290 nm in the ultraviolet region for MHNPs, PEG-MHNPs, and chitosan-MHNPs, respectively (Fig. 3a). The blue shift in the wavelength from 320 nm to 285 nm in the functionalized MHNPs may be attributed to the attachment of polymer molecules, *i.e.* PEG and chitosan with MHNP crystals.[56] The slight variations and appearance of absorption peaks in the band-gap correspond to the band-to-band transition.[57] Fig. 3b shows Tauc's plots, which indicate that the band gap of MHNPs is 3 eV and varied with PEG and chitosan-coated NPs as 2.86 eV and 2.94 eV, respectively. Further optical properties investigation by PL shows two emission peaks at 434 nm and 455 nm in all the cases, *i.e.* bare and polymer-coated MHNPs using an

Table 2 Effect of organic polymers on different structural parameters of MHNPs

| Unit cell parameters | MHNPs | PEG-MHNPs | Chitosan-MHNPs |
|---|---|---|---|
| Crystallite size | 31.3 nm | 23.4 nm | 29.7 nm |
| Lattice cell dimensions | $a$ = 3.149 Å, $c$ = 4.772 Å | $a$ = 3.148 Å, $c$ = 4.771 Å | $a$ = 3.149 Å, $c$ = 4.772 Å |
| Unit cell volume | $4.73 \times 10^{-29}$ m$^3$ | $4.72 \times 10^{-29}$ m$^3$ | $4.73 \times 10^{-29}$ m$^3$ |
| Lattice strain | $1.23 \times 10^{-3}$ | $1.77 \times 10^{-3}$ | $1.31 \times 10^{-3}$ |

Table 3 Texture coefficients of MHNPs, PEG, and chitosan-coated MHNPs

| | | Texture coefficient | | |
|---|---|---|---|---|
| Position ($2\theta$) | Planes | MHNPs | PEG-MHNPs | Chitosan-MHNPs |
| 32.8° | **100** | 0.926 | **1.480** | **1.535** |
| 38° | 011 | 0.927 | 0.810 | 0.840 |
| 50.8° | 012 | 0.874 | 0.879 | 0.780 |
| 58.6° | **110** | **1.262** | 0.829 | 0.842 |

excitation wavelength of 400 nm (Fig. 3c). The emission bands are at the border of the ultraviolet and visible regions and can be attributed to the violet emission. The emission peaks can be attributed to the transition of different $Mg^{2+}$ and $O^{2-}$ states in the magnesium hydroxide's electronic structure.[58] Within the band gap region of the MHNP crystals, the defect states are expected due to the oxygen vacancies.

FTIR spectra are recorded in the range from 650 $cm^{-1}$ to 4000 $cm^{-1}$. In the case of pristine MHNPs, the bands at 652 $cm^{-1}$ and 854 $cm^{-1}$ wavenumbers are attributed to the metal–oxygen bonding. The band at 1422 $cm^{-1}$ indicates the symmetrical–asymmetrical vibrations of the carboxylate O=C=O functional group and 1492 $cm^{-1}$ shows the stretching modes of –OH. Additionally, two bands at 2938 $cm^{-1}$ and 3685 $cm^{-1}$ wave numbers correspond to the out-of-plane bending of C–H and stretching mode of O–H, respectively. It is well established that MgO surfaces when exposed to the atmosphere readily absorb $H_2O$ and $CO_2$ molecules, which results in the formation of MHNPs and the emergence of other functional groups in the FTIR spectrum. In PEGylated MHNPs, there are new bands observed at 1105 $cm^{-1}$, 1342 $cm^{-1}$, and 1607 $cm^{-1}$ which belong to C–O–H, C–H, and C=O bonds, respectively.[59] Whereas in the case of chitosan-coated NPs, C–O–C and C=O bonds are observed at 1046 $cm^{-1}$ and 1572 $cm^{-1}$ wave numbers. The emergence of new bonds confirms the attachment of organic polymers on the surface of the NPs.[60] Fig. 4b represents the hydrodynamic sizes of the pristine and polymer-coated MHNPs. In the case of polymer coating, *i.e.* PEG and chitosan, the average grain size increases as compared to pristine MHNPs. Introducing hydrophilic polymers like PEG and chitosan over the NPs tends to increase the material's hydrodynamic size in liquid due to the formation of hydrated layers, which are linked with the long-chain structure of the polymers.[61] The charged surface of polymer functionalized NPs induces an electrostatic repulsion that helps to limit the further aggregation of NPs and ensure their suspension stability.[62] Therefore, DLS analysis can also confirm the presence of the PEG and chitosan over the MHNPs with the availability of a large number of molecules. The difference in grain size between SEM and hydrodynamic size from DLS can be attributed to the presence of organic molecules *i.e.* PEG and chitosan on the surface of the MHNPs. The increase in the hydrodynamic size of the bare MHNPs is linked with mild aggregation in the solvent and can be overcome by longer ultrasonication time before DLS measurements.

The TGA curves indicate that weight loss for all three nanosystems occurs in different phases (Fig. 4c). Thermal decomposition of the NPs is started soon after the temperature rises; the first weight loss phase is observed below 100 °C, and there is only a 3% weight (inset Fig. 4c) change in the temperature range from 37 to 42 °C, which indicates good water and structural

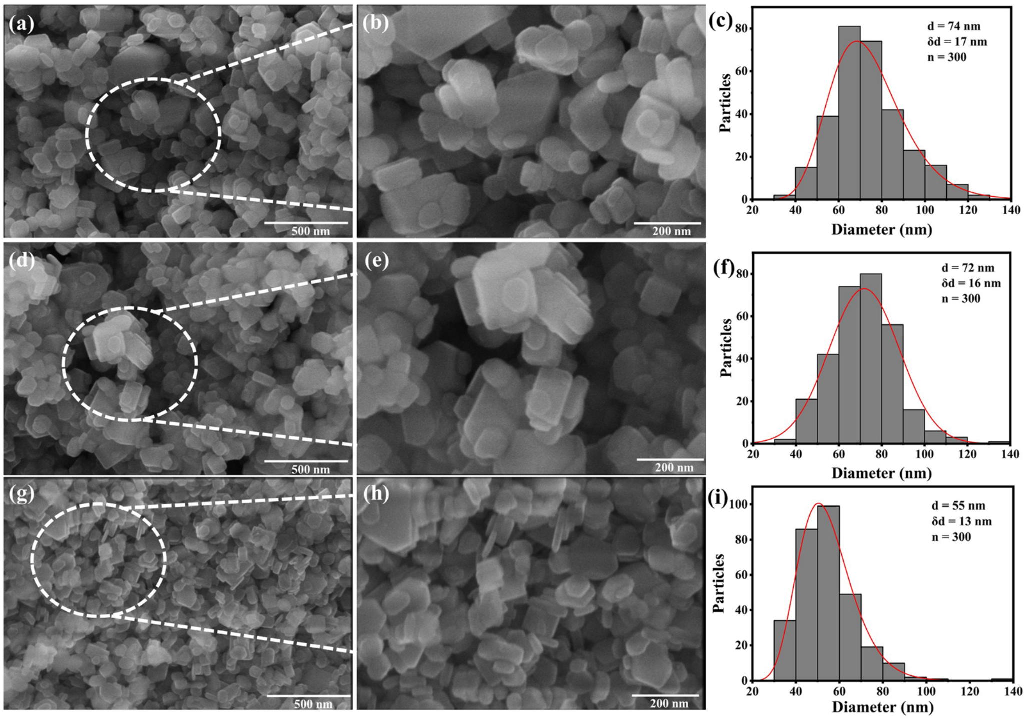

Fig. 2 SEM micrographs at different magnifications and corresponding size distribution histograms:[55] (a)–(c) MHNPs, (d)–(f) PEG functionalized MHNPs, (g)–(i) chitosan coated MHNPs.

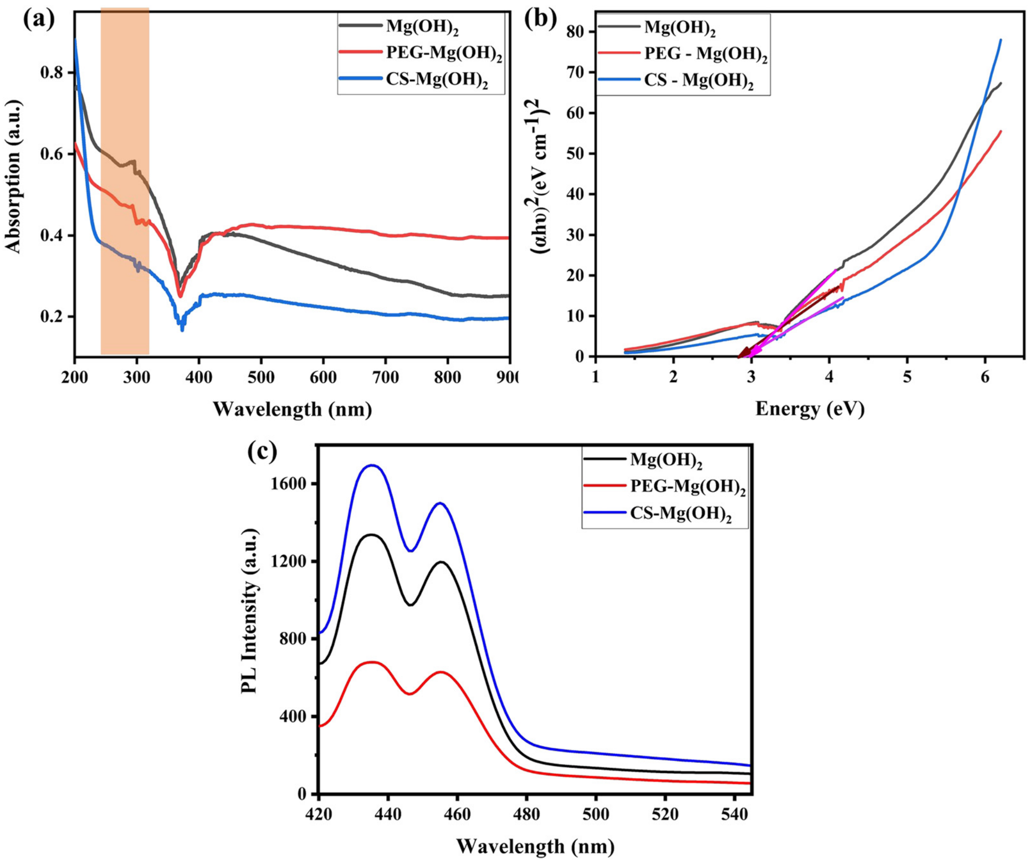

Fig. 3 Optical properties analysis: (a) UV-vis spectra, (b) Tauc's plots for band gap determination, (c) photoluminescence spectra at an excitation wavelength of 400 nm, for MHNPs, PEG-coated MHNPs, and chitosan-coated MHNPs.

retaining ability that can play a crucial role in the antibacterial activity of the bare and functionalized MHNPs by prolonging the interaction with the cell wall of bacteria.[63] For bare MHNPs, the weight loss continues until 300 °C gradually up to 12%. Afterward, 18% weight loss is observed abruptly from 300 °C indicating the removal of absorbed water and decomposition of chemical bonds followed by 8% loss from 600 °C. In the case of PEGylation, there is a gradual weight loss of 20% until 300 °C, and then a further 30% loss is witnessed until 400 °C. In the end, a 12% gradual decrease happened until 750 °C. The chitosan-coated NPs have the least decomposition until 300 °C *i.e.* 8% followed by the decomposition of the MHNPs until 400 °C (32%). Afterward, there is a gradual decrease of 7–8% until the final temperature, *i.e.* 1000 °C. The residual masses of $Mg(OH)_2$, PEG - $Mg(OH)_2$, and chitosan—$Mg(OH)_2$ determined from TGA are 58%, 35%, and 46%, respectively. The first derivative weight loss temperatures are also determined for all the materials and it is observed that this temperature is higher in the case of PEG functionalized MHNPs (367 °C) than bare and chitosan conjugated NPs, that is 321 °C and 316 °C, respectively (Fig. 4d). This also indicates the higher stability of PEG-coated MHNPs than bare and functionalized counterparts.

### 3.2 Antibacterial activity and biofilm inhibition

Before studying the wound healing potential of MHNPs and any potential effects of PEG and chitosan coatings on these properties, it is quite important to evaluate the antibacterial response of all three nano-formulations, as the wounded area is a more exposed and vulnerable site for pathogens to settle down and grow.[64] Therefore, the antibacterial action of MHNPs against *E. coli* and *S. aureus* bacterial strains was studied. The zones of inhibition of the bacterial strains against the nanomaterials are expressed in Table 4 and shown in Fig. 5, which represents that MHNPs have a good antibacterial response and this potential is enhanced by surface functionalization. It is observed that PEG-modified MHNPs perform significantly better against *S. aureus* ($p = 0.001$) whereas *E. coli* is more affected by chitosan-coated MHNPs ($p = 0.002$) (Table 4). Uneven bacterial growth is present in both bacterial strains due to the deployment of biofilms in some regions of the Petri plates. The MHNPs with a size less than 70 nm showed better antibacterial action;[5] firstly, smaller-size MHNPs offer better cellular internalization where they interact with bacterial DNA and other organelles, and secondly, they adsorbed with the bacterial cell wall and release $Mg^{2+}$ ions from the hydroxide structure, which damaged the cell wall.[65,66] Although the precise bactericidal or bacteriostatic mechanism of MHNPs has not yet been elucidated, generally the antibacterial response of NPs is explained by one of these three suggested models; generation of reactive oxygen species, release of metallic ions, and introduction of nonoxidative stress mechanisms.[67] The

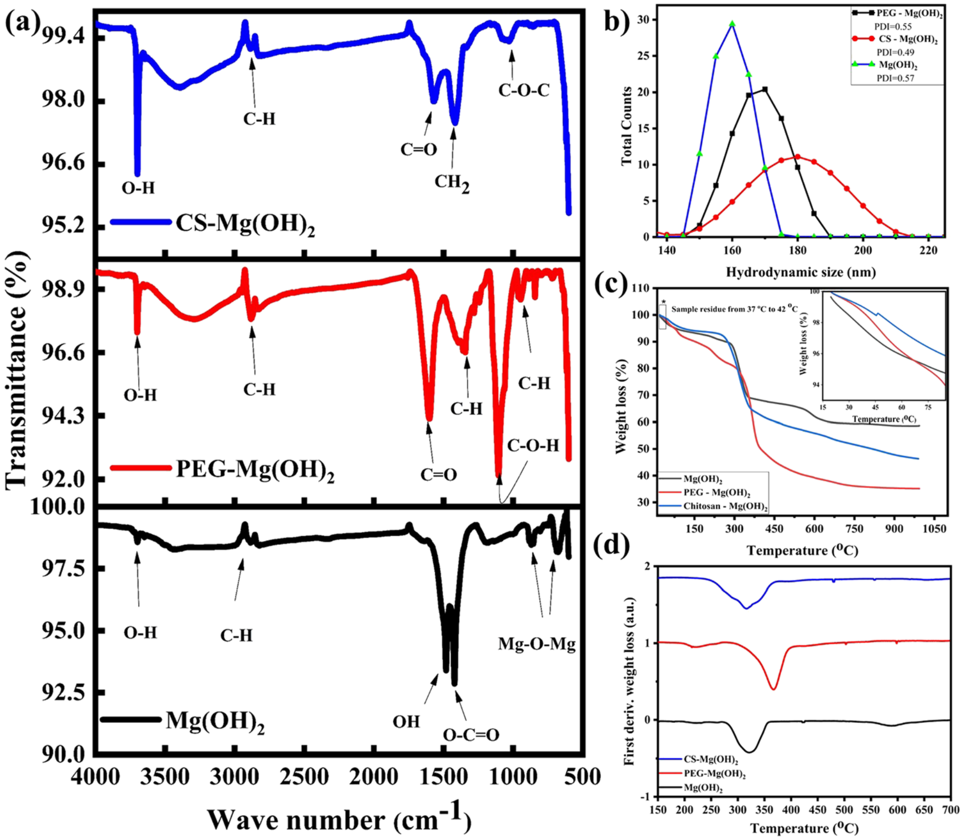

Fig. 4 (a) FTIR, (b) DLS, and (c) TGA profile of bare MHNPs, PEG, and chitosan-coated MHNPs, and (d) first TGA derivative weight loss percentage of MHNPs.

generation of ROS needs $O_2$ as a precursor but MHNPs have shown an antibacterial response even in anaerobic conditions, indicating that the high concentration of $OH^{-1}$ ions can directly damage the cell wall due to electrostatic van der Waals interaction.[30] The ability of MHNP penetration in the cell membrane and protein leakage of *S. aureus* is elevated by increasing the concentration of MHNPs. On attaching to the bacterial surface, MHNPs bind themselves with the cell wall, and the penetrated NPs reduce the metabolic activities by inhibiting protein synthesis.[4] The bound NPs disintegrate the cell wall structure and cause bacterial death by leakage of cellular contents *i.e.* leakage of nucleic acid.[68] The cell walls of *E. coli* and *S. aureus* are composed of a crossed-linked network of peptidoglycan, which is vulnerable to mechanical ruptures, and once this happens, bacteria cannot repair these injuries.[69] This cell wall disintegration can be linked with the alkaline nature of MHNPs with a localized pH value of ≈10. This causes the disturbance of bacterial cellular homeostasis.[70] The alkaline adaptability of *E. coli* and *S. aureus* decreases by increasing the pH value. In the literature, optimum growth of *E. coli* is recorded from weak acidic conditions to neutral (pH 5.6 to 7.0) at 37 °C[71] and *E. coli* remained resistant up to pH 8 whereas above pH 8, inhibition of *E. coli* growth increased (55% at pH 10). Likewise, the growth of *S. aureus* is inhibited 82% at pH ≈ 10 compared to the optimum conditions (pH 6–7) at 30 to 37 °C.

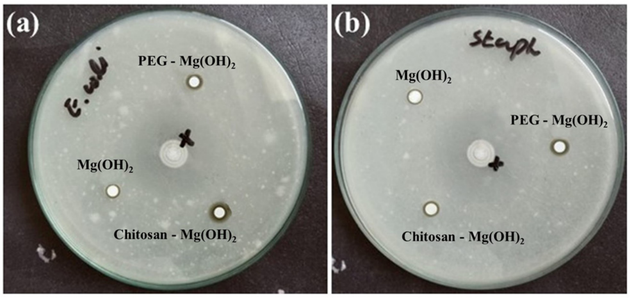

Fig. 5 Zone of inhibition for $Mg(OH)_2$-based nanomaterials of (a) *E. coli*, and (b) *S. aureus*.

Table 4 The zone of inhibition of *E. coli* and *S. aureus* for bare and polymer-coated magnesium hydroxide NPs

| Sample | *E. coli* (ZOI) mm | *S. aureus* (ZOI) mm |
|---|---|---|
| Ciprofloxacin (control) | 30 ± 1 | 26 ± 1 |
| MHNPs | 12 ± 1 | 11 ± 1 |
| PEG-MHNPs | 15 ± 2 | 18 ± 1 |
| Chitosan-MHNPs | 21 ± 2 | 14 ± 3 |

The antibacterial action of MHNPs also lies in their unique hygroscopic nature. This property is enhanced by modifying the surfaces of MHNPs with hygroscopic polymers like PEG and chitosan as evidenced by Table 4 where the inhibition zones are increased when MHNPs are coated with PEG and chitosan. Both PEG and chitosan have an excellent ability to retain water.[72] The conjugation of these polymers with MHNPs increases the adsorption of water molecules on the surface of the MHNPs and forms a very thin moist meniscus due to capillary action. Thus, the MHNPs remain in contact with the bacteria and damage the bacterial membrane, hence, causing cellular destruction.[73,74] PEG and chitosan coatings introduce slightly negative and positive charges respectively on the surface of MHNPs. PEG-coated NPs can develop strong electrostatic interaction with *S. aureus* as compared to *E. coli* and that's why PEG-MHNPs have performed well against $G^+$ rather than $G^-$ bacteria; conversely, due to the appearance of positive charge, chitosan-coated MHNPs are more effective against *E. coli* than *S. aureus*. This electrostatic attraction prolongs the attachment of polymer-coated NPs with bacterial cells and allows invasion from multiple bacterial sites, which reduces the chances to develop resistance against these nanomaterials, consequently causing cell death.

The biofilm inhibition potential of the NPs was also studied for *E. coli* and *S. aureus* bacterial strains. Biofilms are three-dimensional, heterogeneous biopolymer colonial structures of planktonic microorganisms organized on an extracellular polymeric matrix or solid surfaces.[75] This form of bacteria is stable, stress-resistant, and shows great resilience against unfavorable environmental conditions like temperature, drying out, UV exposure, desiccation, and starvation.[76] The formation of a biofilm is due to the development of interconnected complex biochemical aggregation of lipids, proteins, polysaccharides, nucleic acids, and glycol-peptides through maturation, colonization, and adhesion of bacterial cells. In this way, bacterial life organization resembles a multicellular organism and the production of super antigen protein makes it difficult to combat bacteria with traditional antibiotics.[77] The results have shown that PEG and chitosan coatings have increased the inhibition potential of MHNPs for both *E. coli* and *S. aureus* biofilms and from the two polymers, chitosan-coated MHNPs are more effective against *E. coli* and *S. aureus*-based biofilms ($p < 0.0001$) (Table 5). The biofilm formation can be controlled by limiting the surface colonization of bacteria.[78] The biochemical interaction of NPs with biofilms is a step-wise process; (i) introduction of NPs on the biofilm's surface,[79] attachment of NPs to the biofilm's surface, and (iii) penetration of NPs into the biofilms, implemented by physicochemical interaction of NPs, extracellular polymeric matrix and environmental conditions. The surface charge induced due to polymer coating,[80] initially, develops electrostatic attraction with *S. aureus* and *E. coli* and then migrates into the biofilm by diffusion at a different rate. The diffusion rate depends on the size of NPs and the pore size of the biofilm,[81] and smaller-sized NPs diffuse faster; moreover, organic molecules from PEG and chitosan disperse more easily into the biofilm matrix.[82] This shows that the biofilm inhibition ability of MHNPs is improved by surface coating with PEG and chitosan; however, chitosan coating functions slightly better as compared to PEG. The bacterial growth is correlated with the number of microorganisms in the population and the rate of change with respect to time. The optical density (OD) method determines the portion of the light passing through the bacterial suspension. More scattering of light indicates the presence of more bacteria and *vice versa*.[83] It is observed that chitosan-coated MHNPs have statistically significant loss of optical density (less scattering), indicating inhibition of bacteria more efficiently.

### 3.3 Hemolytic activity

To evaluate the potential applicability as a therapeutic agent against complex diseases or in medical implants, it is necessary to test their hemocompatibility before recommending their administration *in vivo*.[43] Hemolytic activity is one of the most fundamental tests that explains the interaction of NPs with blood components; it is an obvious finding of the destruction of RBCs measured by spectroscopic analysis, which causes the discharge of hemoglobin in the body fluids. According to the classification made by the American Society for Testing and Materials (ASTM F 756-00, 2000), materials are categorized into three groups: hemolytic (>5% hemolysis), hemolytic (2–5% hemolysis) and non-hemolytic (<2% hemolysis).[84] Higher hemolytic activity may cause fatal pathological situations. Therefore, determining the *in vitro* and *in vivo* biocompatibility of NPs is a necessary part of preclinical studies. The percentage hemolysis provides the potential of the drug to rupture the cell membrane of erythrocytes[85] and, consequently, indicates cytotoxicity of the injected nanomaterials. The hemolytic activity of pristine and surface-coated MHNPs is given in Table 6. It has been noticed that the percentage hemolysis of MHNPs is reduced when combined with organic polymers *i.e.* from 2.83% to 0.48% and 0.19% for PEG and chitosan, respectively. This indicates higher biocompatibility of polymer surface functionalized MHNPs. Chen *et al.* showed that the size of the NPs is a major contributor to their uptake efficiency, toxic

Table 5 Optical density (OD) and percentage biofilm inhibition of *S. aureus* and *E. coli* for MHNPs and polymer-coated MHNPs

| | Optical density | | | Inhibition (%) | |
|---|---|---|---|---|---|
| Samples | OD control (PBS) | OD *S. aureus* | OD *E. coli* | *S. aureus* | *E. coli* |
| Positive control (Ciprofloxacin) | 0.207 ± 0.001 | 0.013 ± 0.002 | 0.011 ± 0.002 | 93.7 ± 0.3 | 94.7 ± 0.3 |
| MHNPs | 0.207 ± 0.001 | 0.13 ± 0.02 | 0.12 ± 0.02 | 37.2 ± 1.2 | 42.0 ± 2.5 |
| PEG-MHNPs | 0.207 ± 0.001 | 0.10 ± 0.01 | 0.11 ± 0.01 | 51.7 ± 2.7[b] | 46.8 ± 1.3[a] |
| Chitosan-MHNPs | 0.207 ± 0.001 | 0.080 ± 0.01[a] | 0.070 ± 0.01[a] | 61.4 ± 1.1[c] | 66.2 ± 0.5[c] |

[a] Significant. [b] Very significant. [c] Extremely significant.

Table 6 Hemolysis measurements of bare MHNPs, PEG, and chitosan-coated MHNPs

| Materials | Sample absorbance | Hemolysis (%) |
|---|---|---|
| Positive control (Triton X-100) | 1.06 ± 0.00 | 96.41 ± 0.00 |
| Negative control (PBS) | 0.038 ± 0.001 | 0 |
| MHNPs | 0.067 ± 0.003 | 2.83 ± 0.12 |
| PEG-MHNPs | 0.043 ± 0.005[a] | 0.48 ± 0.02[b] |
| Chitosan-MHNPs | 0.040 ± 0.002[b] | 0.19 ± 0.06[b] |

[a] Very significant. [b] Extremely significant.

distribution in the bloodstream, and translocation to different organs as compared to shape, structure, and surface functionalization. This is also consistent with our findings as crystallite size decreases with the introduction of polymers during the synthesis phase of MHNPs.

## 3.4 Wound healing analysis

**3.4.1 CAM assay.** The chorioallantoic membrane[55] is the chick's first respiratory organ formed on the incubation's fourth day. The CAM protects the embryo and helps it to respirate and regulate its metabolism.[79] The CAM assay/model has been used as an alternative *in vivo* model and follows the 3R principle (reduction, replacement, and refinement) in animal experiments. The wound healing investigation using the CAM assay shows that controls have no significant changes and eggs remain in their initial stage as evident from Fig. 6a and b, whereas NPs (MHNPs, PEG-MHNPs, chitosan-MHNPs) incorporated alginate gels present proper ongoing growth of the chicks in all cases (Fig. 6(c)–(e)). In the case of NPs modified gels, the formation of blood vessels is prominent, and the heartbeat of the chick was observed to be normal and the yolks are completely changed into living bodies (chick). Magnesium hydroxide-based nanomaterials form some sort of scaffold over the cut part of the eggs that stops the evaporation of the internal fluid, which helps in maintaining homeostasis and continues the growth; consequently, the intentional wound can be healed. These results suggested that the presence of the magnesium hydroxide NPs in the alginate gel can enhance the wound healing potential of the gel. This is a very unique study and no such study is reported in the literature where NPs modified alginate gels have been studied.

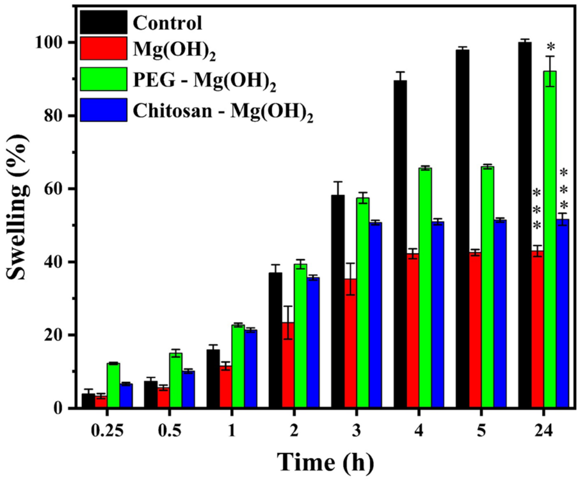

Fig. 7 Swelling behavior of NP-modified alginate gel for 24 h (control = alginate gel only). *Significant, ***extremely significant.

Keeping the wound bed moist and clean is the most important condition that promotes the healing process, especially in the case of open wounds.[86] The hygroscopic nature of MHNPs

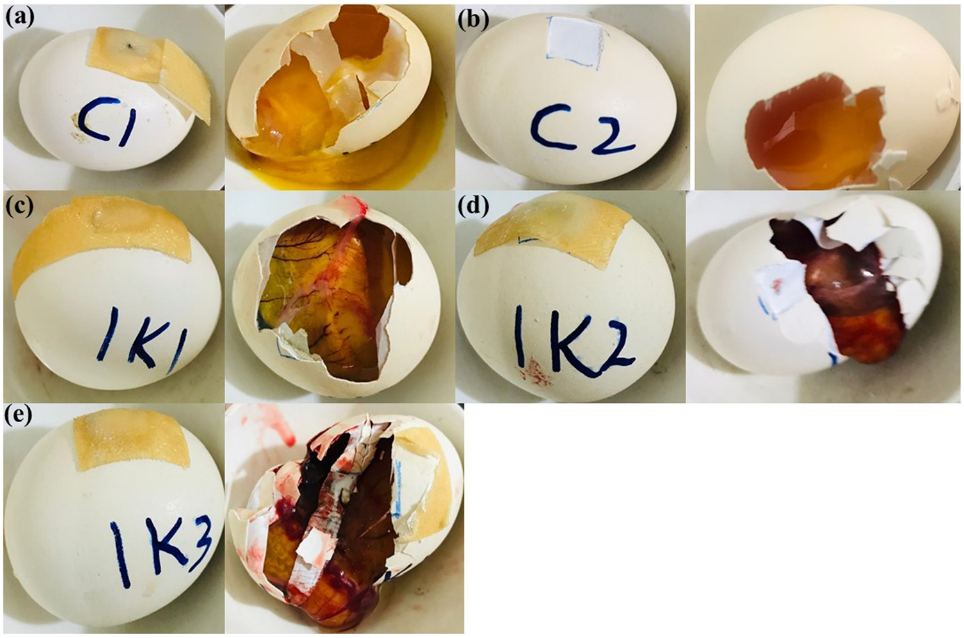

Fig. 6 Wound healing using CAM assay; (a) C1 = Alginate gel, (b) C2 = No alginate gel, (c) 1K1 = MHNPs, (d) 1K2 = PEG-coated MHNPs, (e) 1K3 = chitosan coated MHNPs.

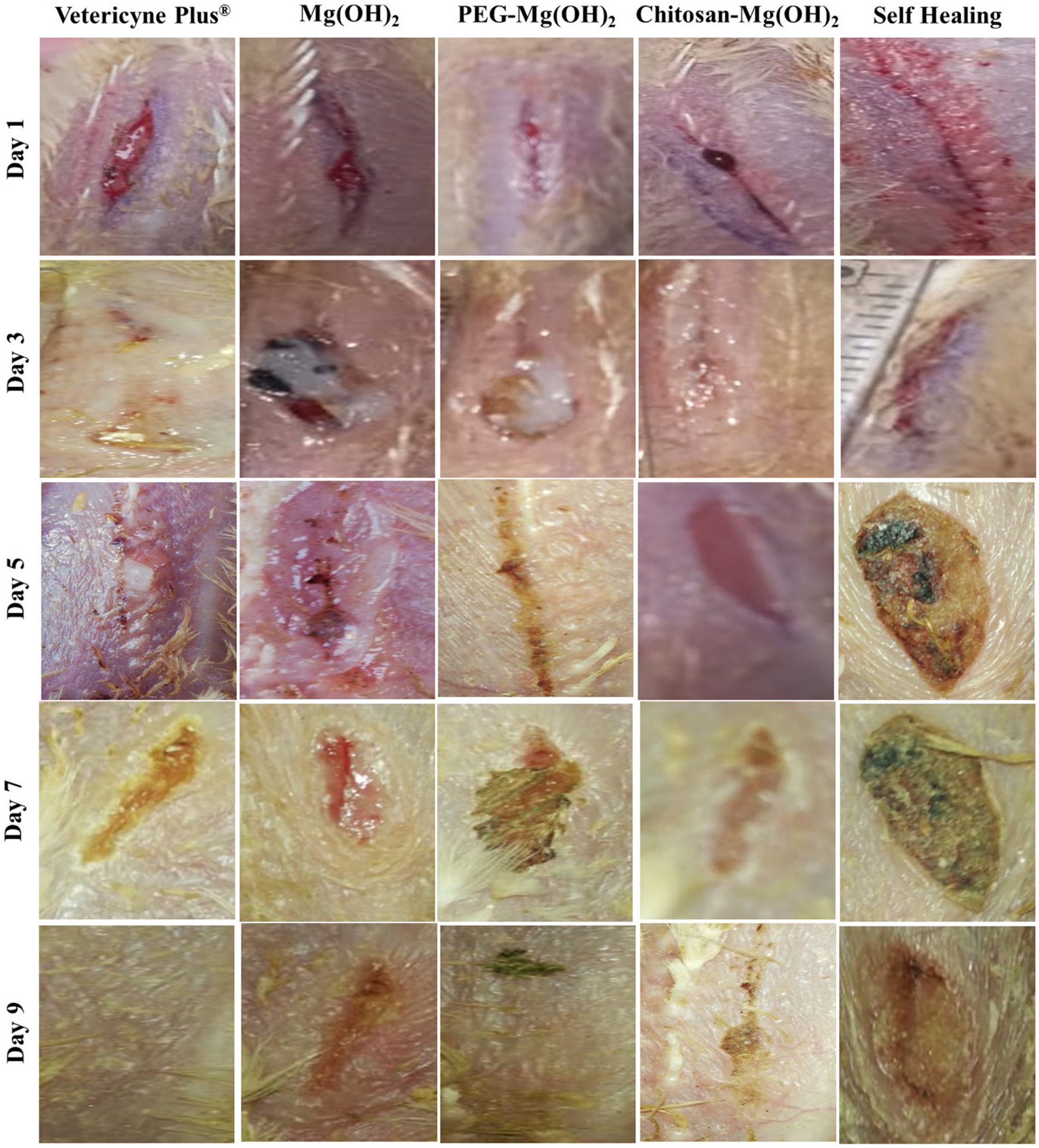

Fig. 8 Photographic analysis of wound healing on the 1st, 3rd, 5th, 7th, and 9th day after incision on *G. domesticus*.

can be useful in absorbing wound exudates and keeping the wound bed clean, which is usually achieved by ointments. The antibacterial potential of magnesium hydroxide can additionally safeguard the wound from airborne infectious bacteria.[87] The swelling behavior of bare and polymer-coated magnesium hydroxide NPs incorporated into the gel is also observed by investigating their ability to absorb water content. It can be observed from Fig. 7 that the swelling behavior of the alginate gel is affected by the addition of NPs. Alginate gel has a higher swelling percentage and this is reduced by the addition of NPs on the gel. From three composite gels, the gel incorporated with the pristine MHNPs has the lowest swelling percentage, whereas, in the case of polymer coatings, *i.e.* PEG and chitosan, the swelling percentage is increased indicating the role of the polymer over the surface of the MHNPs. Alginate gel containing PEGylated MHNPs swelled relatively more over time ($p < 0.0001$) than the chitosan-functionalized MHNP modified gel. The swelling saturation in the gels is observed for up to 5 h, and afterward remains the same for 24 h.

**3.4.2 Would healing on *G. domesticus*.** Wound healing is a complicated and continuous process, completed in different phases (hemostasis, inflammation, cell proliferation, and maturation), which are sequential and overlapped.[84] The wound healing is observed by creating an open type of wound on *Gallus gallus domesticus* for 9 d. Different groups of animals as mentioned in Table 1 show distinct effects on the healing rate (Fig. 8 and 9a). Fig. 8 shows a pictorial representation of the healing process at different stages with respect to time (Day 1 to day 9). It

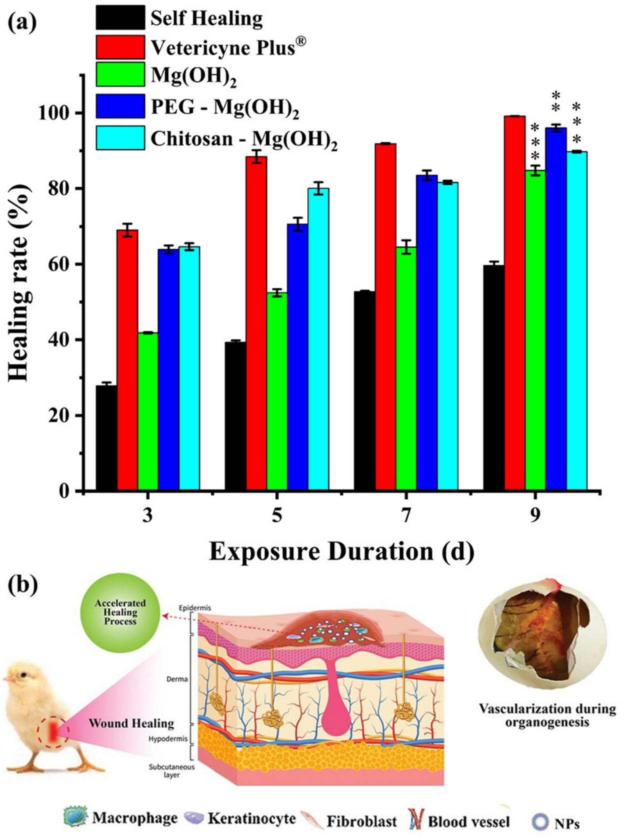

Fig. 9 (a) Wound healing analysis in terms of healing rate (%) on the 3rd, 5th, 7th and 9th day. **Very significant, ***extremely significant, (b) skin remodeling process.

can be seen that 99% of the wound is healed by Vetericyne Plus® and no scarring indication over the wounded area. Bare and chitosan-coated MHNPs have shown a slower healing process until day 9. Minute scarring can still be visualized on the wounds in the case of bare and chitosan-functionalized MHNPs. However, the healing response of PEG-coated MHNPs is very significant and the appearance of the skin looks good with negligible scarring whereas the natural recovery of the wound is very slow and the state of the skin does not look good. Although the wound is closed, a scar is quite prominent over the wound bed indicating the ongoing skin remodeling phase.[88]

Fig. 9a indicates the percentage of wound healing based on the changes that occurred in the wounds as compared to the state of the wounds on the first day. PEGylated MHNPs and chitosan-coated MHNPs have shown promising potential to close and heal wounds as compared to pristine MHNPs. The wound healing % for bare MHNPs is 41.83 ± 0.17%, 52.44 ± 0.9%, 64.56 ± 1.78%, and 84.77 ± 1.26% for the 3rd, 5th,7th, and 9th day, respectively, whereas, in the case of polymer coating, the healing rate is increased significantly for PEGylated MHNPs, and it is 63.93 ± 1.06%, 70.62 ± 1.7%, 83.49 ± 1.27% and 96.04 ± 0.89% and 64.65 ± 0.91%, 80.03 ± 1.63%, 81.60 ± 0.43% and 89.76 ± 0.2% for chitosan-coated MHNPs. MHNPs are currently used as antacids that can be useful for avoiding bed sores during the healing phase. However, the role of Mg (trace element) in wound healing is still not well defined.[89] Pollack has discussed that trace elements like Mg can be useful in the wound-healing process.[90] Pastorfide *et al.* found that the application of MHNPs ointment on the wounds of obstetrical patients is very safe and accelerates wound healing.[91] Lange *et al.* explained that Mg cations can promote wound healing due to their ability to promote β1 integrin-mediated adhesion of dermal fibronectin and migration of keratinocytes to different extracellular matrix proteins.[92] Chitosan is a naturally bioactive polymer; the ability of protonation of amino groups with the polysaccharide network of chitosan enabled its solubility in an acidic medium, whereas depolymerization of chitosan into *N*-acetyl-D-glucosamine gradually triggers the fibroblast proliferation, helps in orderly deposition of collagen and initiates the synthesis of hyaluronic acid at the wound bed. The positively charged chitosan-coated MHNPs might have aggregated with the negatively charged erythrocytes, platelets, and fibrinogen, and this electrostatic interaction facilitates blood hemostasis.[21] As we have discussed in the earlier section the coating of chitosan has increased the

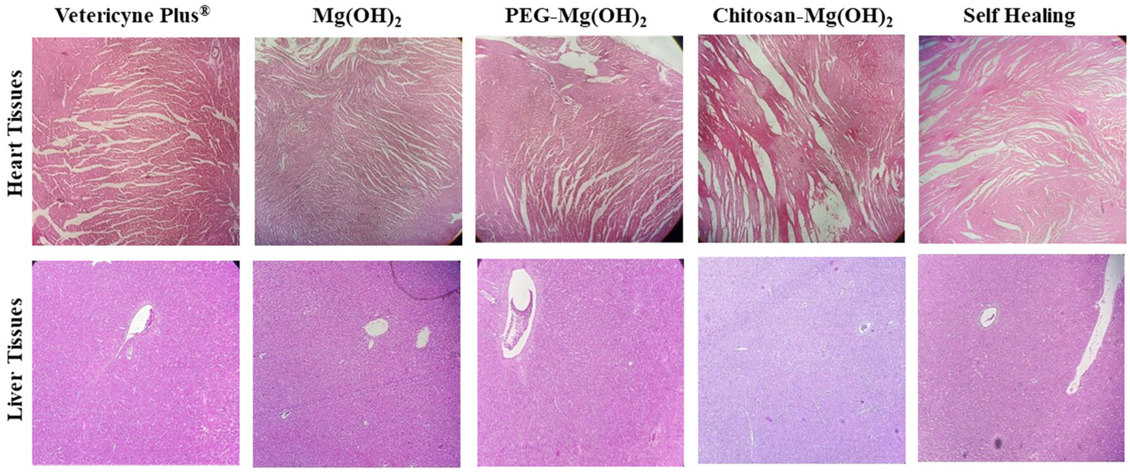

Fig. 10 Histopathological micrographs of heart and liver tissues of *G. domesticus* treated with MHNPs.

antibacterial response of MHNPs, and therefore enhanced antibacterial potential might have inhibited the growth of bacteria over the wound bed, prevented inflammation and infection, and also increased the healing process (Fig. 9b). Chen *et al.* showed that the nontoxic nature of PEG promotes reepithelization when open wounds are treated with PEGylated systems. The appearance of a scar on the skin is very common during the wound healing phase; although the collagen composition of the scar cells is similar to the cells it replaces, there is a difference in the fiber composition of the protein. The scar tissues are affected by the fibrinolysis and fibrinogenesis balance. In normal healthy tissues collagen fibers obtain randomly formed basket weave structures while in fibrosis, fibers cross-link and align themselves in one particular direction.[93] As PEG decreases the toxicity and increases the retention time of NPs,[39] the wounds treated with PEGylated MHNPs show improved healing and the skin regenerates its normal texture (Fig. 8) and shows that it has the potential to heal the wounds. Less inflammation and negligible scarring are due to the antibacterial response and better tissue adhesion ability of PEGylated MHNPs. Our results suggest that the MHNPs coated with bioactive, nontoxic, and biodegradable polymers like PEG and chitosan can be included in wound healing ointments.

### 3.5 Toxico-patho-biochemistry examination

To investigate any toxicity induced by the magnesium hydroxide NPs in the case of absorption into the bloodstream, the complete hematological examination and blood serum biochemistry profile of *Gallus gallus domesticus* were evaluated. The values of red blood cells, white blood cells, hemoglobin, and platelet count are normal in all groups with negligible variations (Table S1, ESI†). Blood and serum biochemistry analysis (Table S2, ESI†) indicates that blood glucose, uric acid, blood urea, serum triglyceride, and serum cholesterol are normal. However, there is a minute increase in the alanine aminotransferase,[45] which is also known as serum glutamic-pyruvic transaminase (SGPT), of those chicks that are treated with pristine and polymer-coated MHNPs that indicates a slight variation in the liver functioning which is not considered malfunctioning, high-density lipoprotein (HDL) value, and histopathology shows that the liver is functioning normally. So there are no toxic effects and major variations observed in the blood and serum of chicks.[94] All the readings are statistically analyzed by two-way ANOVA followed by Tukey's test and significance is accepted at $p < 0.05$.

Fig. 10 also indicates that there are no residual toxic effects seen on the heart tissues of the chicks. All the cardiac myocytes are normal, inflammation and necrosis are not seen and there is no sign of fatty change and cellular atypia. Similarly, the livers of all the chicks are normal and functioning well, hepatocytes are normal and are surrounded by a central vein and there is no indication of fat deposition or inflammation in the liver tissues. Liver parenchymal changes and high vascularity are not observed, which ruled out the possibility of tumor formation.[95] These results have shown that MHNPs in the pristine state and particularly coated with PEG and chitosan induced no intoxication on the organs and can be recommended for use in wound healing recipes for fast recovery.

## 4. Conclusion

Surface-modified MHNPs, particularly PEG, have accelerated the healing of skin wounds of *Gallus gallus domesticus*. No toxic effects were observed in blood and serum composition. Histopathological examination of the liver and heart has also confirmed the normal state of these organs. The size reduction due to polymer coating helped the cellular internalization and increased the stability at lower temperatures which enhanced the antibacterial action against bacterial strains. The biofilm inhibition potential of chitosan functionalized magnesium hydroxide NPs was 66.10% and 61.36% against *E. coli* and *S. aureus*, respectively. These findings indicate that surface-modified MHNPs, specifically PEGylated NPs, are safe to use in the case of minor dermal injuries/cuts of birds and can be extended to treat mammalian skins.

## Author contributions

MKA: methodology, formal analysis, writing – original draft, YJ: conceptualization, supervision, resources, writing – review and editing, NAS: resources, formal analysis, writing – review and editing, MS: resources, data curation, BA: validation, writing – review and editing, EY: methodology, data curation, SKS: writing – review and editing, NTKT: funding acquisition, data analysis, writing – critical review and editing.

## Data availability

The data supporting this article have been included as part of the ESI.†

## Conflicts of interest

The authors have no conflict to declare.

## References

1 S. Zhang, *et al.*, Antimicrobial properties of metal nanoparticles and their oxide materials and their applications in oral biology, *J. Nanomater.*, 2022, 2063265.

2 F. Aflakian, *et al.*, Nanoparticles-based therapeutics for the management of bacterial infections: a special emphasis on FDA approved products and clinical trials, *Eur. J. Pharm. Sci.*, 2023, 106515.

3 Y. Wang, *et al.*, Surface-functionalized design of blood-contacting biomaterials for preventing coagulation and promoting hemostasis, *Friction*, 2023, **11**(8), 1371–1394.

4 Y. Zhu, *et al.*, $Mg(OH)_2$ nanoparticles enhance the antibacterial activities of macrophages by activating the reactive oxygen species, *J. Biomed. Mater. Res., Part A*, 2021, **109**(11), 2369–2380.

5 A. F. Halbus, T. S. Horozov and V. N. Paunov, Controlling the antimicrobial action of surface modified magnesium hydroxide nanoparticles, *Biomimetics*, 2019, **4**(2), 41.

6 Y. Luo, *et al.*, Size controlled fabrication of enzyme encapsulated amorphous calcium phosphate nanoparticle and its intracellular biosensing application, *Colloids Surf., B*, 2021, **201**, 111638.

7 G. Unnikrishnan, *et al.*, PVA–CS polymeric system conjugated with GO–ZnO–Ag 2 O ternary composite–a multifunctional nanocomposite for wound healing applications, *New J. Chem.*, 2024, **48**(19), 8908–8925.

8 H. Liao, *et al.*, An intrinsically self-healing and anti-freezing molecular chains induced polyacrylamide-based hydrogel electrolytes for zinc manganese dioxide batteries, *J. Energy Chem.*, 2024, **89**, 565–578.

9 J. Yuan, *et al.*, Biomimetic peptide dynamic hydrogel inspired by humanized defensin nanonets as the wound-healing gel coating, *Chem. Eng. J.*, 2023, **470**, 144266.

10 M. Zhao, *et al.*, Stem Cell-Derived Nanovesicles Embedded in Dual-Layered Hydrogel for Programmed ROS Regulation and Comprehensive Tissue Regeneration in Burn Wound Healing, *Adv. Mater.*, 2024, 2401369.

11 C.-A. Cheng, *et al.*, A responsive mesoporous silica nanoparticle platform for magnetic resonance imaging-guided high-intensity focused ultrasound-stimulated cargo delivery with controllable location, time, and dose, *J. Am. Chem. Soc.*, 2019, **141**(44), 17670–17684.

12 H. Huang, *et al.*, One-step fabrication of PEGylated fluorescent nanodiamonds through the thiol-ene click reaction and their potential for biological imaging, *Appl. Surf. Sci.*, 2018, **439**, 1143–1151.

13 M. Matsumoto, M. Matsusaki and M. J. Mb Akashi, Preparation of biodegradable peptide nanospheres with hetero PEG brush surfaces, *Macromol. Biosci.*, 2014, **14**(1), 142–150.

14 B. Yin, *et al.*, Intrapulmonary cellular-level distribution of inhaled nanoparticles with defined functional groups and its correlations with protein corona and inflammatory response, *ACS Nano*, 2019, **13**(12), 14048–14069.

15 L. Shi, *et al.*, Effects of polyethylene glycol on the surface of nanoparticles for targeted drug delivery, *Nanoscale*, 2021, **13**(24), 10748–10764.

16 C. P. Jiménez-Gómez and J. A. Cecilia, Chitosan: a natural biopolymer with a wide and varied range of applications, *Molecules*, 2020, **25**(17), 3981.

17 S. M. Dadou, *et al.*, Effect of protonation state and N-acetylation of chitosan on its interaction with xanthan gum: a molecular dynamics simulation study, *Mar. Drugs*, 2017, **15**(10), 298.

18 K. Azuma, *et al.*, Chitin, chitosan, and its derivatives for wound healing: old and new materials, *J. Funct. Biomater.*, 2015, **6**(1), 104–142.

19 G. Unnikrishnan, *et al.*, Preparation and characterizations of antibacterial and electroactive polymeric composites for wound healing applications, *Polym. Compos.*, 2024, **45**(1), 267–285.

20 H. Nosrati, *et al.*, Nanocomposite scaffolds for accelerating chronic wound healing by enhancing angiogenesis, *J. Nanobiotechnol.*, 2021, **19**(1), 1–21.

21 S. Ahmed and S. Ikram, Chitosan based scaffolds and their applications in wound healing, *Achiev. Life Sci.*, 2016, **10**(1), 27–37.

22 M. Liu, *et al.*, Incorporation of magnesium oxide nanoparticles into electrospun membranes improves pro-angiogenic activity and promotes diabetic wound healing, *Biomater. Adv.*, 2022, **133**, 112609.

23 U. Mamat, *et al.*, Detoxifying Escherichia coli for endotoxin-free production of recombinant proteins, *Microb. Cell Fact.*, 2015, **14**, 1–15.

24 M. M. Dinges, P. M. Orwin and P. M. Schlievert, Exotoxins of Staphylococcus aureus, *Clin. Microbiol. Rev.*, 2000, **13**(1), 16–34.

25 K. Ou, *et al.*, Covalently grafting polycation to bacterial cellulose for antibacterial and anti-cell adhesive wound dressings, *Int. J. Biol. Macromol.*, 2024, **269**, 132157.

26 S. Ghildiyal, *et al.*, Wound healing and antimicrobial activity of two classical formulations of Laghupanchamula in rats, *J. Ayurveda Integr. Med.*, 2015, **6**(4), 241.

27 J. cQu, *et al.*, Hybrid nanocomposite multinetwork hydrogel containing magnesium hydroxide nanoparticles with enhanced antibacterial activity for wound dressing applications, *Polymer*, 2022, **251**, 124902.

28 D. Chen, *et al.*, Key difference between transition state stabilization and ground state destabilization: increasing atomic charge densities before or during enzyme–substrate binding, *Chem. Sci.*, 2022, **13**(27), 8193–8202.

29 Y. Liu, *et al.*, Fabrication and research of $Mg(OH)_2$/PCL/PVP nanofiber membranes loaded by antibacterial and biosafe $Mg(OH)_2$ nanoparticles, *Polym. Test.*, 2022, **112**, 107635.

30 Y. Meng, *et al.*, Antimicrobial activity of nano-magnesium hydroxide against oral bacteria and application in root canal sealer, *Med. Sci. Monit.: Int. Med. J. Exp. Clin. Res.*, 2020, **26**, e922920–1.

31 M. Rajkumar, *et al.*, Green synthesis of gelatin-loaded magnesium hydroxide nanocomposite biomaterial using Coleus amboinicus leaf extract for enhanced antibacterial, antioxidant, anticholinergic, and wound healing activities, *J. Mater. Res.*, 2024, **39**(4), 548–564.

32 J. Tan, *et al.*, Effect of local alkaline microenvironment on the behaviors of bacteria and osteogenic cells, *ACS Appl. Mater. Interfaces*, 2018, **10**(49), 42018–42029.

33 H. Qin, *et al.*, Anti-biofilm properties of magnesium metal via alkaline pH, *RSC Adv.*, 2015, **5**(28), 21434–21444.

34 A. Hoshino, *et al.*, Physicochemical properties and cellular toxicity of nanocrystal quantum dots depend on their surface modification, *Nano Lett.*, 2004, **4**(11), 2163–2169.

35 A. Alimohammad, *et al.*, A study of the effect of magnesium hydroxide on the wound healing process in rats, *Med. J. Islamic World Acad. Sci.*, 2006, **16**(4), 165–170.

36 S. Alizadeh, *et al.*, Enhancing Diabetic Wound Healing Through Improved Angiogenesis: The Role of Emulsion–Based Core–Shell Micro/Nanofibrous Scaffold with Sustained CuO Nanoparticle Delivery, *Small*, 2024, 2309164.

37 R. R. Al-Ajeli, A.-H. M. Al-Hasan and S. S. Al-Mahmood, The Role of Magnesium Oxide Nanoparticles In The Healing

Process of Cervical Esophageal Anastomosis in Dogs: An Experimental study, *Egypt. J. Vet. Sci.*, 2022, **53**(4), 547–557.

38 S. Shi, *et al.*, High-Fidelity End-Functionalization of Poly (ethylene glycol) Using Stable and Potent Carbamate Linkages, *Angew. Chem., Int. Ed.*, 2020, **59**(41), 18172–18178.

39 T. L. Lasseter, *et al.*, Covalently modified silicon and diamond surfaces: resistance to nonspecific protein adsorption and optimization for biosensing, *J. Am. Chem. Soc.*, 2004, **126**(33), 10220–10221.

40 D. Jin, *et al.*, Hydrothermal synthesis and characterization of hexagonal Mg (OH) 2 nano-flake as a flame retardant, *Mater. Chem. Phys.*, 2008, **112**(3), 962–965.

41 J. Hudzicki, *Kirby-Bauer disk diffusion susceptibility test protocol*. American society for microbiology, 2009. vol. 15, pp. 55–63.

42 M. K. Abbas, *et al.*, Polyethylene glycol dictates the therapeutic response (anticancer and wound healing) of silver oxide nanomaterials, *Polym. Adv. Technol.*, 2023, **34**(8), 2606–2619.

43 W. Zhou, *et al.*, Synthesis and hemolytic activity of magnesium hydroxide nanoparticles, *Adv. Mater. Res.*, 2014, **971–973**, 228–231.

44 M. A. Dobrovolskaia, *et al.*, Method for analysis of nanoparticle hemolytic properties in vitro, *Nano Lett.*, 2008, **8**(8), 2180–2187.

45 M. Zahid, *et al.*, Development of hydrogels with the incorporation of Raphanus sativus L. seed extract in sodium alginate for wound-healing application, *Gels*, 2021, **7**(3), 107.

46 I. Liakos, *et al.*, Fibrous wound dressings encapsulating essential oils as natural antimicrobial agents, *J. Mater. Chem. B*, 2015, **3**(8), 1583–1589.

47 A. Krajca and R. Juranova, Anesthesia in poultry, *Vet. Med.*, 1994, **39**(1), 23–27.

48 H. Zhao, *et al.*, Function of Chick Subcutaneous Adipose Tissue During the Embryonic and Posthatch Period, *Front. Physiol.*, 2021, **12**, 684426.

49 W. Zhang, *et al.*, Preparation of $Mg(OH)_2$ nanosheets and self-assembly of its flower-like nanostructure via precipitation method for heat-resistance application, *Integr. Ferroelectr.*, 2015, **163**(1), 148–154.

50 P. Wang, *et al.*, Morphology control and growth mechanism of magnesium hydroxide nanoparticles via a simple wet precipitation method, *Ceram. Int.*, 2011, **37**(8), 3365–3370.

51 R. G. Sibbald, *et al.*, Bacteriology, inflammation, and healing: a study of nanocrystalline silver dressings in chronic venous leg ulcers, *Adv. Skin Wound Care*, 2007, **20**(10), 549–558.

52 A. Ullah, *et al.*, Mechanistic insight of dye degradation using TiO2 anchored α-MnO2 nanorods as promising sunlight driven photocatalyst, *Mater. Sci. Eng., B*, 2021, **271**, 115257.

53 S. Thanikaikarasan, *et al.*, Characterization of electroplated FeSe thin films, *J. Mater. Sci.: Mater. Electron.*, 2009, **20**, 727–734.

54 S. Yousefi, *et al.*, Optical properties of MgO and $Mg(OH)_2$ nanostructures synthesized by a chemical precipitation method using impure brine, *J. Alloys Compd.*, 2017, **711**, 521–529.

55 N. Fleitas-Salazar, *et al.*, Effect of temperature on the synthesis of silver nanoparticles with polyethylene glycol: new insights into the reduction mechanism, *J. Nanopart. Res.*, 2017, **19**(3), 113.

56 R. De Silva, *et al.*, Nano-MgO reinforced chitosan nanocomposites for high performance packaging applications with improved mechanical, thermal and barrier properties, *Carbohydr. Polym.*, 2017, **157**, 739–747.

57 P. Tyagi and A. Vedeshwar, Grain size dependent optical band gap of $CdI_2$ films, *Bull. Mater. Sci.*, 2001, **24**, 297–300.

58 S. Yousefi, B. Ghasemi and M. Tajally, PEG-assisted synthesis and formation mechanism of Mg (OH) 2 nanostructures using natural brine, *Appl. Phys. A*, 2020, **126**, 1–11.

59 M. H. Zahir, *et al.*, Shape-stabilized phase change materials for solar energy storage: MgO and $Mg(OH)_2$ mixed with polyethylene glycol, *Nanomaterials*, 2019, **9**(12), 1773.

60 M. Barzegar, *et al.*, Green synthesis of magnesium oxide nanoparticles by chitosan polymer and assessment of their photocatalytic activity and cytotoxicity influences, *Mater. Chem. Phys.*, 2023, **301**, 127649.

61 A. C. Makan, *et al.*, Advanced analysis of polymer emulsions: Particle size and particle size distribution by field-flow fractionation and dynamic light scattering, *J. Chromatogr. A*, 2016, **1442**, 94–106.

62 Z. Rajabimashhadi, *et al.*, Novel Synthesis of Nano Mg (OH) 2 by Means of Hydrothermal Method with Different Surfactants, *Nanomaterials*, 2023, **13**(3), 454.

63 X. Li, Y. Zhao and C. Zhao, Applications of capillary action in drug delivery, *iScience*, 2021, **24**(7), 102810.

64 V. Puca, *et al.*, Microbial species isolated from infected wounds and antimicrobial resistance analysis: Data emerging from a three-years retrospective study, *Antibiotics*, 2021, **10**(10), 1162.

65 N. M. Franklin, *et al.*, Comparative toxicity of nanoparticulate ZnO, bulk ZnO, and $ZnCl_2$ to a freshwater microalga (Pseudokirchneriella subcapitata): the importance of particle solubility, *Environ. Sci. Technol.*, 2007, **41**(24), 8484–8490.

66 M. Heinlaan, *et al.*, Toxicity of nanosized and bulk ZnO, CuO and $TiO_2$ to bacteria Vibrio fischeri and crustaceans Daphnia magna and Thamnocephalus platyurus, *Chemosphere*, 2008, **71**(7), 1308–1316.

67 V. Karunagaran, K. Rajendran and S. Sen, Optimization of biosynthesis of silver oxide nanoparticles and its anticancer activity, *Int. J. Nanosci.*, 2017, **16**(05n06), 1750018.

68 X. Pan, *et al.*, Investigation of antibacterial activity and related mechanism of a series of nano-$Mg(OH)_2$, *ACS Appl. Mater. Interfaces*, 2013, **5**(3), 1137–1142.

69 J. C. Gumbart, *et al.*, Escherichia coli peptidoglycan structure and mechanics as predicted by atomic-scale simulations, *PLoS Comput. Biol.*, 2014, **10**(2), e1003475.

70 A. Truskewycz, *et al.*, Fluorescent magnesium hydroxide nanosheet bandages with tailored properties for biocompatible antimicrobial wound dressings and pH monitoring, *ACS Appl. Mater. Interfaces*, 2021, **13**(24), 27904–27919.

71 P. Philip, *et al.*, Parallel substrate supply and pH stabilization for optimal screening of E. coli with the membrane-based fed-batch shake flask, *Microb. Cell Fact.*, 2018, **17**(1), 1–17.

72 M. Nadir, I. Ansyar and P. Khaerani. Effect of various polyethylene glycol concentrations on the growth of seedlings of Indigofera zollingeriana, *IOP Conference Series: Earth and Environmental Science*, IOP Publishing, 2019.

73 A. Pilarska, *et al.*, Functional polypropylene composites filled with ultra-fine magnesium hydroxide, *Open Chem.*, 2014, **13**(1), 000010151520150024.

74 H. Li, *et al.*, pH-responsive eco-friendly chitosan–chlorella hydrogel beads for water retention and controlled release of humic acid, *Water*, 2022, **14**(8), 1190.

75 S. C. Chew, *et al.*, Dynamic remodeling of microbial biofilms by functionally distinct exopolysaccharides, *mBio*, 2014, **5**(4), e01536–14.

76 R. M. Donlan, Biofilm formation: a clinically relevant microbiological process, *Clin. Infect. Dis.*, 2001, **33**(8), 1387–1392.

77 S. T. Asma, *et al.*, An overview of biofilm formation–combating strategies and mechanisms of action of antibiofilm agents, *Life*, 2022, **12**(8), 1110.

78 L. Shkodenko, I. Kassirov and E. Koshel, Metal oxide nanoparticles against bacterial biofilms: Perspectives and limitations, *Microorganisms*, 2020, **8**(10), 1545.

79 D. Oliinyk, *et al.*, Chorioallantoic membrane assay at the cross-roads of adipose-tissue-derived stem cell research, *Cells*, 2023, **12**(4), 592.

80 E. Fröhlich, The role of surface charge in cellular uptake and cytotoxicity of medical nanoparticles, *Int. J. Nanomed.*, 2012, 5577–5591.

81 E. Sahle-Demessie and H. Tadesse, Kinetics and equilibrium adsorption of nano-TiO2 particles on synthetic biofilm, *Surf. Sci.*, 2011, **605**(13–14), 1177–1184.

82 C. Boyoglu, *et al.*, The intracellular co-localizations of different size of gold nanoparticles, *Nanotechnology*, 2011, 489–492.

83 K. Stevenson, *et al.*, General calibration of microbial growth in microplate readers, *Sci. Rep.*, 2016, **6**(1), 1–7.

84 D. Archana, *et al.*, Chitosan-PVP-nano silver oxide wound dressing: in vitro and in vivo evaluation, *Int. J. Biol. Macromol.*, 2015, **73**, 49–57.

85 M. A. Dobrovolskaia and S. E. McNeil, Understanding the correlation between in vitro and in vivo immunotoxicity tests for nanomedicines, *J. Controlled Release*, 2013, **172**(2), 456–466.

86 J. P. Junker, *et al.*, Clinical impact upon wound healing and inflammation in moist, wet, and dry environments, *Adv. Wound Care*, 2013, **2**(7), 348–356.

87 X.-Y. Wang, *et al.*, Experimental and first-principle computational exploration on biomass cellulose/magnesium hydroxide composite: Local structure, interfacial interaction and antibacterial property, *Int. J. Biol. Macromol.*, 2021, **191**, 584–590.

88 G. C. Gurtner, *et al.*, Wound repair and regeneration, *Nature*, 2008, **453**(7193), 314–321.

89 C. L. Wetteland, *et al.*, Dissociation of magnesium oxide and magnesium hydroxide nanoparticles in physiologically relevant fluids, *J. Nanopart. Res.*, 2018, **20**, 1–17.

90 S. V. Pollack, Wound healing: a review: III. Nutritional factors affecting wound healing, *J. Dermatol. Surg. Oncol.*, 1979, **5**(8), 615–619.

91 G. Pastorfide, *et al.*, Zinc chloride spray-magnesium hydroxide ointment dual topical regimen in the treatment of obstetric and gynecologic incisional wounds, *Clin. Ther.*, 1989, **11**(2), 258–263.

92 T. S. Lange, *et al.*, $Mg^{2+}$ and $Ca^{2+}$ differentially regulate β1 integrin-mediated adhesion of dermal fibroblasts and keratinocytes to various extracellular matrix proteins, *Exp. Cell Res.*, 1994, **214**(1), 381–388.

93 S.-L. Chen, *et al.*, A PEG-based hydrogel for effective wound care management, *Cell Transplant.*, 2018, **27**(2), 275–284.

94 C. U. Nwaigwe, *et al.*, Evaluation of the hematological and clinical biochemical markers of stress in broiler chickens, *Vet World*, 2020, **13**(10), 2294–2300.

95 A. Khan, *et al.*, Arsenic Toxicity in Broiler Chicks and its Alleviation with Ascorbic Acid: A Toxico-patho-biochemical Study, *Int. J. Agric. Biol.*, 2013, **15**, 1105–1111.